Atmos. Chem. Phys. Discuss., 13, 26001–26041, 2013
www.atmos-chem-phys-discuss.net/13/26001/2013/
doi:10.5194/acpd-13-26001-2013

Atmospheric Chemistry and Physics Discussions

Changes in atmospheric aerosol loading retrieved from space based measurements during the past decade

J. Yoon[1,*], J. P. Burrows[1], M. Vountas[1], W. von Hoyningen-Huene[1], D. Y. Chang[2], A. Richter[1], and A. Hilboll[1]

[1]Institute of Environmental Physics, University of Bremen, Bremen, Germany
[2]Atmospheric Chemistry Department, Max-Planck-Institute for Chemistry, Mainz, Germany
[*]now at: Max-Planck-Institute for Chemistry, Mainz, Germany

Received: 17 June 2013 – Accepted: 6 September 2013 – Published: 9 October 2013

Correspondence to: J. P. Burrows (burrows@iup.physik.uni-bremen.de)

Published by Copernicus Publications on behalf of the European Geosciences Union.

Abstract

Atmospheric aerosol, generated from natural and anthropogenic sources, plays a key role in regulating visibility, air quality, and acid deposition. It is directly linked to and impacts on human health. It also reflects and absorbs incoming solar radiation and thereby influences the climate change. The cooling by aerosols is now recognized to have partly masked the atmospheric warming from fossil fuel combustion emissions. The role and potential management of short-lived climate pollutants such as aerosol are currently a topic of much scientific and public debate. Our limited knowledge of atmospheric aerosol and its influence on the Earth's radiation balance has a significant impact on the accuracy and error of current predictions of the future global climate change. In the past decades, environmental legislation in industrialized countries has begun to limit the release of anthropogenic pollutants. In contrast, in Asia as a result of the recent rapid economic development, emissions from industry and traffic have increased dramatically. In this study, the temporal changes/trends of atmospheric aerosols, derived from the satellite instruments MODIS (on board Terra and Aqua), MISR (Terra), and SeaWiFS (OrbView-2) during the past decade, are investigated. Whilst the aerosol optical thickness, AOT, over Western Europe decreases (i.e. by up to about −40 % from 2003 to 2008) and parts of North America, a statistically significant increase (about +34 % in the same period) over East China is observed and attributed to both the increase in industrial output and the Asian desert dust.

1 Introduction

Anthropogenic aerosol from both fossil fuel combustion and land use change is now well known to impact on human health and global climate change. Detailed knowledge of long-term temporal changes of local, regional, and global aerosols is needed to test our scientific understanding of its sources and sinks and to provide an evidence base for policymakers (World Meteorological Organization (WMO), 2011; World

ACPD
13, 26001–26041, 2013

Health Organization (WHO) 2012; Solomon et al., 2007; Climate and Clean Air Coalition (CCAC), 2012; Richter et al., 2005). As a result of remarkable advances in technology over the last decades, the observations from remote sensing instrumentation on Earth orbiting satellite platforms now provide novel and unique global information about atmospheric aerosols (e.g., Advanced Very High Resolution Radiometer (AVHRR), Total Ozone Mapping Spectrometer (TOMS), Along Track Scanning Radiometer (ATSR) Multi-angle Imaging SpectroRadiometer (MISR), Moderate Resolution Imaging Spectroradiometer (MODIS), and Sea-viewing Wide Field-of-view Sensor (SeaWiFS)) (Li et al., 2009; Thomas et al., 2010; Yu et al., 2009; Zhang and Reid, 2010; Karnieli et al., 2009; Mishchenko et al., 2007; Mishchenko and Geogdzhayev, 2007; Zhao et al., 2008; Massie et al., 2004; Yoon et al., 2011; Hsu et al., 2012; de Meij et al., 2012). In particular the aerosol products from the sensors, MODIS, MISR and SeaWiFS are often used because of their relatively long-term observation periods, stable and accurate sensor calibration, and the validated, quantified and high accuracies of the aerosol retrieved data products.

The unrepresentative sampling of polar-orbiting platforms in time and space is a limitation for the change and trend analysis as discussed elsewhere (Li et al., 2009; Ignatov et al., 2005; Kahn et al., 2007; Levy et al., 2009; Yoon, et al., 2011, 2012), and will remain partially unresolved until an adequate "fit for purpose" measurement system is established, replacing the experimental series of satellite instrumentation currently in space. The issue arises because of the different sampling times (e.g., local equatorial crossing times are 10:30 a.m. for Terra, 12:20 p.m. for OrbView-2, and 01:30 p.m. for Aqua), limited orbital period (i.e., roughly 100 min for each orbit), and frequent cloud contamination or disturbance i.e. from the small and wispy sub pixel clouds, which are challenging to separate from aerosol.

In this study, the changes and trends of atmospheric aerosol have been determined from the retrieved AOT data from MODIS (Terra and Aqua), MISR (Terra), and SeaWiFS (OrbView-2) during the past 15 years. We firstly minimized the uncertainty caused by the unrepresentative sampling using the relevant polar orbiting satellites observa-

ACPD
13, 26001–26041, 2013

tions and weighted least squares regression (Thomas et al., 2010; Yoon, et al., 2012). The selection criteria for data from the different sensors in the trend analysis include the duration of the observation periods (National Aeronautics and Space Administration (NASA), MODIS Web, 2000; Jet Propulsion Laboratory – NASA, MISR Multiangle Imaging SpectroRadiometer, 2000; Goddard Space Flight Center – NASA, SeaWiFS Project, 1997; The International Ocean-Colour Coordinating Group (IOCCG), 2011) and the stability and accuracy of the sensor calibration (Kahn et al., 2005a; Bruegge et al., 2007; Li et al., 2009; Barnes et al., 2001; Gordon, 1998; Eplee et al., 2001). Overall relatively high accuracies for the AOT retrievals (Kaufman et al., 1997; Remer et al., 2005, 2008; Levy et al., 2010; Kahn et al., 2005b, 2010; von Hoyningen-Huene et al., 2003, 2006, 2011; Yoon et al., 2011) and their merged trends are obtained. More detailed information about the instrument and satellite platform characteristics, calibration status, AOT retrieval accuracy, and research data are summarized in Table 1.

2 Regions and datasets

The average values of the AOT derived using the retrieval algorithms, developed for the independent instruments MODIS (Terra) from March 2000 to December 2009, MISR (Terra) from March 2000 to December 2010, SeaWiFS (OrbView-2) from January 1998 to December 2007, and MODIS (Aqua) from January 2003 to December 2008, are shown in Fig. 1. Ten regions are selected for more detailed investigation in Europe, Middle/Near East, Asia, and North America and include large urban agglomerations. Recently changes in aerosol, resulting from both direct emissions from fossil fuel combustion and the secondary aerosol created by photochemical transformations of trace gases, have been reported in these regions (Streets et al., 2003; Zhao et al., 2008). In addition, the aerosol, downwind from deserts, is influenced by wind-blown mineral dust (Zhao et al., 2008; Yoon et al., 2012).

ACPD
13, 26001–26041, 2013

2.1 MODIS, on NASA Terra (March 2000–December 2009) and NASA Aqua (January 2003–December 2008)

The Moderate-Resolution Imaging Spectroradiometers (MODIS) (NASA, MODIS Web, 2000; The International Ocean-Colour Coordinating Group (IOCCG), 2011) on the Terra and Aqua spacecrafts have contributed uniquely to our knowledge of atmospheric aerosols over the last decade. The first MODIS instrument is mounted on NASA Terra, which was launched on 18 December 1999. The second instrument, mounted on NASA Aqua spacecraft, started to observe global aerosols on 4 May 2002. The main objective of these instruments is to improve our understanding of global dynamics and processes occurring on land, in the oceans, and in the lower atmosphere. They achieve global coverage every one to two days. The MODIS instruments have been well calibrated (~ 2 % absolute and ~ 1 % precision) (Li et al., 2009) using on-board, vicarious, and lunar targets. Their data yield aerosol products having high accuracy (±0.05 or ±15 % over land and ±5 % over ocean for AOT) (Kaufman et al., 1997; Remer et al., 2005, 2008; Levy et al., 2010) suitable for trend analysis. Their monthly AOTs at 550 nm and cloud fraction (CF) from Level 3 Collection 5 global products (1° × 1° spatial resolution) are used in this study.

2.2 MISR (NASA Terra, March 2000–December 2010)

The Multiangle Imaging SpectroRadiometer (MISR) (Jet Propulsion Laboratory – NASA, MISR Multiangle Imaging SpectroRadiometer, 2000; IOCCG, 2011) instrument, one of the sensors on-board the Terra spacecraft, provides Earth viewings in the visible wavelength range simultaneously at nine widely spaced angles. This unique feature enables different types of atmospheric aerosols, clouds, and land surface covers to be distinguished. In addition, the instrument provides global coverage at high spatial resolution (i.e. 275 m × 275 m, 275 m × 1.1 km, 1.1 km × 1.1 km), but it takes around nine days to cover the entire Earth surface. The sensor is carefully calibrated (~ 3 % absolute, 1–2 % channel-to-channel relative, 1 % precision) (Kahn et al., 2005a; Bruegge

ACPD
13, 26001–26041, 2013

et al., 2007) using on-board, vicarious, and lunar targets. In this study, monthly AOTs at 558 nm (±0.05 or ±20 % over land and ocean) (Kahn et al., 2005b, 2010) from Level 3 Component Global Aerosol Product version F15 (CGAS-F15) products (0.5° × 0.5° spatial resolution) are used.

2.3 SeaWiFS (NASA OrbView-2, January 1998 to December 2007)

The Sea-viewing Wide Field Sensor (SeaWiFS) (Goddard Space Flight Center – NASA, SeaWiFS Project, 1997; IOCCG, 2011) on OrbView-2, launched in August 1997, continuously measured Earthshine radiances, which were well calibrated (accuracy: 0.5 % and stability: 0.3 %) (Li et al., 2009; Barnes et al., 2001; Gordon, 1998; Eplee et al., 2001) using on-board, lunar, and vicarious calibration procedures. In this study, SeaWiFS Level 1B Global-Area Coverage data (L1B GAC) are used for AOT retrieval over selected regions using the Bremen AErosol Retrieval (BAER) algorithm (von Hoyningen-Huene et al., 2003, 2006, 2011). It has been demonstrated that the AOT error of BAER retrievals ranges within ±0.05 or ±20–25 % over land and ocean (von Hoyningen-Huene et al., 2011; Yoon et al., 2011). The trends of atmospheric aerosols are analysed in this study using monthly AOTs at 510 nm from Level 3 Global Product with 1° × 1° spatial resolution.

2.4 AERONET (AErosol RObotic NETwork)

The AERONET is a global network of ground-based instruments (i.e. sun photometers) for monitoring aerosol optical properties and validating the aerosol products retrieved from satellite borne measurements. It provides long-term records of cloud-free AOT (Remer et al., 1997; Dubovik et al., 2002) with high temporal resolution as well as high retrieval accuracy (Holben et al., 1998, 2001; Eck et al., 1999). In this study, Level 2.0 AERONET AOTs are used not only for validation of AOT trends retrieved from the satellites but also to test uncertainty or error caused by temporal sampling limitations.

ACPD
13, 26001–26041, 2013

3 Different/limited temporal sampling of polar-orbiting satellites

The reduction of the error and uncertainty in the trend analysis of cloud-free AOT, retrieved from measurements of the upwelling solar and thermal infrared spectrum by instruments on polar-orbiting satellite, is achieved by a variety of approaches. This includes optimization of instrument calibration and the refinement of retrieval algorithms (Zhao et al., 2008; Karnieli et al., 2009; Mishchenko et al., 2007; Mishchenko and Geogdzhayev, 2007; Massie et al., 2004; Hsu et al., 2012; de Meij et al., 2012). Thus far, no study has fully addressed the issue of the unrepresentative sampling, induced by different/limited temporal sampling of the instruments (Li et al., 2009; Yoon et al., 2011; Ignatov et al., 2005; Kahn et al., 2007; Levy et al., 2009). Adequate sampling is a prerequisite for deriving reliable and representative trends. An advantage of the polar-orbiting satellite data used in this study is their global coverage, but they are limited in the continuous temporal observations at a given location.

The temporal pattern correlations between different samplings (at 10:30 a.m. ± 30 min for Terra, 12:20 p.m. ± 30 min for OrbView-2, and 01:30 p.m. ± 30 min for Aqua, and all available samplings) were investigated using monthly AERONET AOTs at 550 nm, which are determined from the retrieved AOTs at 440 nm by using knowledge of the Ångström exponent for the 440–675 nm region. Since there is no difference in retrieval accuracy, cloud filtering method, and spatial resolution for each station, the differences in the temporal pattern correlations from this investigation are caused only by the different and limited sampling. The AERONET stations were selected using the criterion that the minimum temporal length of the data set is five years (see Yoon et al., 2012).

Figure 2 shows the Taylor diagrams, which describe three statistical metrics in one plot, viz. temporal correlation, normalized standard deviation, and normalized centred root-mean-square (RMS) difference of the two time series (Taylor, 2001; Solomon et al., 2007; Meehl et al., 2007), for the temporal pattern correlation between the monthly AERONET AOTs resampled at the local equatorial crossing times

ACPD
13, 26001–26041, 2013

of the instruments used in this study: 10:30 a.m. ± 30 min, 12:20 p.m. ± 30 min, and 01:30 p.m. ± 30 min. The AERONET stations used in Fig. 2 are classified by their regional dominant aerosol types, e.g. industrial/biomass burning, free troposphere, desert dust, and rural aerosols, and listed on Table 2. The aerosol classification is explained in Yoon et al. (2012). At the stations influenced by desert and rural aerosols, the temporal pattern correlation is obtained for all the times of sampling ($0.91 \leq$ temporal $R \leq 0.98$, $0.87 \leq$ normalized temporal STD ≤ 1.13, and $0.19 \leq$ normalized centred RMS difference ≤ 0.44). In contrast, the correlation at the stations where industrial/biomass burning and free tropospheric aerosols are dominant, is poorer i.e. $0.72 \leq$ temporal $R \leq 0.94$, $0.78 \leq$ normalized temporal STD ≤ 1.21, and $0.36 \leq$ normalized centred RMS difference ≤ 0.80. As there is no difference in retrieval accuracy, cloud-filtering method, and spatial resolution as mentioned before, this difference is attributed only to the different and limited sampling times, which are related to diurnal variation of the aerosol sources (Smirnov et al., 2002). In particular, the temporal correlation coefficient at the station Beijing ranges from 0.72 to 0.83, and there is good chance of deriving different trends from the different/limited samplings over such a large urban agglomeration. This knowledge is needed to understand the difference in the AOT trends from the different/limited temporal sampling of the satellite data.

To minimize the impact of different/limited sampling on the determination of the trend, the present study analyses global AOT trends derived from multiple polar orbiting satellites observations: Terra (MODIS and MISR), OrbView-2 (SeaWiFS), and Aqua (MODIS).

4 Weighted trend model for considering cloud disturbance

To derive an accurate and reliable change/trend analysis of atmospheric AOTs, the impact of sub scene cloud needs to be considered. The insufficient number of AOT retrieval induced by thin or wispy clouds in the instrument field of view causes a bias in the trend analysis since it is a significant influence on the statistical representative-

ACPD
13, 26001–26041, 2013

ness of monthly AOT means (Yoon et al., 2011). Generally, cloud occurrence causes the decrease of observation number (n_t). A relatively large spatial standard deviation compared to the mean (σ_t/y_t) is a good indicator for cloud contamination in cloud-free AOT retrieval (Yoon et al., 2011). Therefore, the combination of these parameters as a weighting factor yields a minimum impact of cloud contamination on the change/trend analysis of cloud-free global AOT (Yoon et al., 2012), and is used in this study. The monthly AOTs (y_t) are used for fitting the linear regression where R^2 is minimized by

$$R^2(A,B) = \sum_{t=1}^{T} \left(wt_t \times \left(y_t - A - Bx_t - \tilde{y}^m \right) \right)^2 \quad (1)$$

where, wt_t is the monthly weighting factor ($\sqrt{n_t}/\left(\sigma_t/y_t\right)$), t is time in months ($t = 1 \ldots T$), A is a constant term, B is the magnitude of the trend per year ($x_t = t/12$), n_t is the total number of observations per month, y_t is the monthly AOT measurement, σ_t is the standard deviation of the monthly AOTs. $\tilde{y}^m$ represents the total mean of y_t (i.e. the climatological monthly varying pattern in AOT) for each month ($m = 1 \ldots 12$) and accounts for the seasonal/natural AOT cycle in the trend estimation.

Figure 3 shows the simple linear and weighted changes/trends, as well as total means and standard deviations of cloud fraction (CF), derived from MODIS (Terra) products (March 2001 ~ December 2009). The simple linear and weighted trends shown in Fig. 3a and b, are generally consistent. However, in terms of the intensity and tendency, significant differences are found predominantly over regions having large CF variability in Fig. 3c, e.g.:

(i) A clear spatial division of the AOT trends in Fig. 3a is found near coastal locations, i.e. across the land sea boundary, even though they have a common dominant aerosol source from the land. The pattern of increasing trends over the Indian subcontinent is often different across its land and ocean boundaries;

(ii) There is no positive signal over Brazil even though it is one of the BRICs (a group of the countries: Brazil, Russia, India, and China having advanced economic development (Goldman Sachs, 2003)). In spite of efforts to diminish the impact of

ACPD
13, 26001–26041, 2013

slash and burn deforestation since 2001 in Brazil, significant amounts of aerosol and NO_x are produced by this activity;

(iii) The simple linear AOT trends over South Africa and Southeast Asia show a clear discontinuity between land and surrounding ocean areas.

These findings are indicative of either instrumental (e.g. platform characteristics, sensor calibration etc.), or retrieval (AOT retrieval accuracy), or sampling or atmospheric (changes resulting from human activity or natural phenomena) issues. As mentioned above, one important systematic source of error for trend analysis of cloud-free AOT is attributed to cloud disturbance. Thus the trend analysis is expected to be less robust over regions, where frequent cloud occurrence persists throughout the year as shown in Fig. 3c and d e.g., most of the marine areas and tropical rain/cloud forests in the equatorial zone.

For the problematic regions, mentioned above, the differences in AOT at coasts are reduced in the weighted trend compared to that of the simple linear trend. The discontinuities of the MODIS-Terra AOT trend between land and ocean over South Asia, Southeast Asia, South Africa has disappeared, and a positive trend is now found over South America in Fig. 3b. Over the majority of the ocean, a continuous cloud disturbance results in unrepresentative sampling all year around as shown in Fig. 3c and d, and the derivation of statistically significant AOT trends over oceans is limited by this issue. Consequently, for the regional trend analysis of cloud-free AOT, the present study focuses on those regions, which are not significantly influenced by cloud disturbance as selected and shown in Fig. 1.

4.1 Outlier tests of the weighting factors

To remove outliers from the weighting factors we use the Grubbs test (Grubbs, 1969) and a Gaussian test within 95 % of confidence levels. Firstly, the Grubbs test is used to detect outliers in weighting factors using the assumption that an approximately normal

ACPD
13, 26001–26041, 2013

distribution is the most probable distribution.

$$G_t > (N-1)/N\sqrt{t^2_{(\alpha/N,N-2)}/\left(N-2+t^2_{(\alpha/N,N-2)}\right)} \quad \text{with} \quad G_i = (wt_i - \mu_{wt})/\sigma_{wt} \tag{2}$$

where, N, μ_{wt}, and σ_{wt} are the total number, total mean, and total standard deviation of wt_i, respectively. $t^2_{(\alpha/N,N-2)}$ denotes the critical value of the t-distribution with $(N-2)$ degrees of freedom and a significance level of (α/N). If the weighting factor satisfies Eq. (2), it is rejected as an outlier. After removing outliers by using the Grubbs test, the remaining weighting factors follow a Gaussian distribution. In a second step, the hypothesis about no outliers within approximately 95 % of confidence level is discarded if wt_t satisfies the following Eq. (3):

$$wt_t > \mu_{wt} + 2\sigma_{wt} \quad \text{or} \quad wt_t < \mu_{wt} - 2\sigma_{wt} \tag{3}$$

Using these statistical tests and assumptions, outliers are successfully removed in the weighted trend analysis. Figure 4 illustrates an example of the outlier tests for significant weighting factors.

4.2 Significance test of the weighting trends

For a meaningful analysis of regional AOT trends, the present study takes into account the weighted trend (B_g) for each grid cell ($1^\circ \times 1^\circ$ for MODIS and SeaWiFS or $0.5^\circ \times 0.5^\circ$ for MISR) with significance ($|B_g/\sigma_{B_g}|$) larger than two, from which it can be concluded that the trend is significant within 95 % confidence level (Weatherhead et al., 1998; Zhao et al., 2008; Yoon et al., 2011). The standard deviation of the gridded trend (σ_{B_g}) is estimated using the bootstrap method (Mudelsee, 2010) (aka, Monte Carlo error bars analysis), using 5000 resampling iterations of monthly AOT anomalies for each grid.

ACPD
13, 26001–26041, 2013

5 Trend validation with AERONET observation

The aerosol retrievals from different cloud masking approaches in the various algorithms can lead to different monthly, seasonal, and annual behaviours, and thereby influence the trend analysis. To minimize the cloud uncertainty, a weighted trend approach is introduced in this study. In addition there is another important source of difference in trends arising from the different temporal sampling, as discussed above and demonstrated in Fig. 2.

The trend for each of the satellite AOT data products has been validated by comparing it with that available from the AERONET stations, listed in Table 3. Figure 5 shows the scatterplots and correlation analysis. The AERONET stations are selected by the criteria of having three years or more of the continuous observation. The three-years time span may be insufficiently short for the trend estimation, but it is practical for the trend validation over global area. Since the AERONET monthly AOT is calculated from all available sampling with high temporal resolution and accuracy (Holben et al., 1998, 2001; Eck et al., 1999), the AOT trends derived from satellite observations are expected to be different against the AERONET AOT trends at least due to different and limited sampling times as discussed in Fig. 2. In summary, from this comparison we can show how much different the satellite-derived trends are against the AERONET AOT trends, "actual trends".

In Fig. 5a and b, the AERONET AOT trend shows better correlation with the MODIS (Terra) trend than with the MISR trend. This is partly explained by MISR having a smaller swath width and spatial coverage, even though MODIS and MISR are onboard the same space platform, Terra. However MISR provides the only valuable trends over desert regions in this study. This is because the MISR algorithm retrieves AOT over these highly reflecting surfaces using its multiple-viewing observations (Kahn et al., 2007, 2010). The weighted trends of the SeaWiFS/BAER AOT and that of the AERONET AOT are generally in good agreement having high correlation ($R = 0.8$) in Fig. 5c. However, the low slope of the SeaWiFS trends compared to that of AERONET

ACPD
13, 26001–26041, 2013

might be attributed to either an underestimation of SeaWiFS AOT (up to 20 % near heavily polluted areas as a result of absorbing aerosols) (von Hoyningen-Huene et al., 2011), an OrbView-2 orbital drift (about two hours delay till end of 2007) (Yoon et al., 2011), or the strict cloud-filtering method applied in BAER (von Hoyningen-Huene et al., 2011; Yoon et al., 2011). In contrast, the weighted trends of MODIS (Aqua) and AERONET AOTs have a higher slope of 0.7, but somewhat poorer correlation ($R = 0.6$) with AEONET, as shown in Fig. 5d. Overall and taking into account any biases introduced by their different sampling times and limited orbital periods, it can be concluded that the AOT trends derived from satellite- and ground-based observations are correlated ($0.4 \leq R \leq 0.9$).

6 Regional trend analysis

Figure 6 shows the significances of weighted trends. In this study, statistically significant trends within 95 % confidence level are used for the regional trend analysis. The significant trends determined using a linear-weighted regression for each of the data sets, shown in Fig. 7, are different depending on the instruments. One significant reason for these differences is attributed to the difference in temporal sampling of the instruments as discussed.

In Fig. 8 the AOT trends shown for the regions 1 to 10 are estimated from the data products from each of the individual instruments. In Western Europe, region 1 in Fig. 1, AOT from industry and traffic sources decreases significantly (Marmer et al., 2007; Karnieli et al., 2009). This is attributed to the success of environmental regulation in the EU countries (Streets et al., 2003; Yoon et al., 2011, 2012; Hilboll et al., 2013). Over Eastern Europe, region 2, large emissions of smoke aerosols from summer peat and forest fires and industrial pollutants from urban areas have been reported during the measurement period (Richter et al., 2005; Hayn et al., 2009; Yoon et al., 2011). However overall, AOT also decreases in this region. This more complex behaviour is a result of societal changes initiated within Perestroika in the 1980's and the subse-

ACPD
13, 26001–26041, 2013

quent political and economic practices in Eastern Europe in the 1990's. These then in turn produced changes in the vehicle fleet and industrial practices. Overall emissions have been reduced. However, a significant temporal increase of MODIS (Aqua) AOT is observed in the afternoon. In this context, positive trends of NO_2 emissions (Zhou et al., 2012; Streets et al., 2006) over Eastern Europe in the afternoon have been identified and similarly burned areas from Global Fire Emissions Database (GFED) (Giglio et al., 2010) over Eastern Europe, as shown in Fig. 9 for the period 2004 to 2008 are increasing.

The cities of the Near/Middle East, such as Cairo, having a combination of increasing population, intense fossil fuel combustion and poorly regulated vehicle emissions, exhibit some of the highest local air pollution levels known. In addition mineral dust from the Saharan and Arabian deserts, dependent the prevailing wind direction, is an aerosol type, on which pollutants deposit, over the Near/Middle East (Sabbah et al., 2006; Zhao et al., 2008; Yoon et al., 2012), region 3 in Fig. 1. Significant amounts of fine-mode aerosols, produced by the petroleum industry and related shipping, are also observed (Basart et al., 2009; Yoon et al., 2012). MISR AOTs are the only available data and thereby they provide more representative mean of significant trends over the bright desert areas in this study as shown from blue bar chart of significant trend pixels in Fig. 8. The trend in the Near/Middle East shows a significant increase. This is explained by an increase of coarse-mode aerosols from deserts (Yoon et al., 2012) and of fine-mode aerosols from oil production, refining and other industry in and around the Red Sea and the Persian Gulf (Sadrinasab and Kämpf, 2004). Emissions from fossil fuel combustion by shipping passing through the Suez Canal and Red Sea (Franke et al., 2009; Richter et al., 2004; de Ruyter de Wildt et al., 2012) also play a role.

The aerosol over the Indian sub-continent, as shown in region 4 in Fig. 1, is increasing. AOT is influenced by a variety of emission sources (Dey et al., 2004; Ramanathan et al., 2007a,b): fossil fuel combustion, domestic burning of biofuels, biomass burning, forest fires, mineral dust, and maritime aerosol. Significant AOT increases are observed in all the data sets during the observation period. The recent rapid economic growth

ACPD
13, 26001–26041, 2013

in India, where GDP increased (The World Bank Group, 2012) by ∼ 7.5 % annually from 1998 to 2010, coupled with the second largest and growing population of the world, which is around 1.2 billion, with nearly ∼ 1 billion people living in and around the Ganges valley, are factors contributing to the significant enhancement in the release of aerosol and its precursors.

Regions 5–7 in China show markedly increasing AOT. The Chinese economy is the second largest in the world (about $7.3 trillion of GDP in 2011 (The World Bank Group, 2012) and had annual growth rates (The World Bank Group, 2012) of ∼ 10 % or more over the past decade. Moreover, China is the world's most populous country, having a growing population of more than 1.35 billion people. As a consequence of the growth of industry, related construction and changes of land usage, large amounts of aerosol and their precursors are emitted into the atmosphere (Zhao et al., 2008; Yoon et al., 2012) in the conurbations of China. Additionally, mineral dust from the Asian deserts is transported by the predominantly westerly winds in spring and summer into this region, prior to its transport into the Pacific and the amount is increasing (Zhang et al., 2003; Yoon et al., 2012). The visibility in China is well known to be poor and AOTs over China during the period of observation have significantly increased (Streets et al., 2003, 2006; Mishchenko and Geogdzhayev, 2007; Zhao et al., 2008; Yoon et al., 2012). The AOT trend over region 8 (Korea and Japan), located in the same belt of westerly winds, shows consistently an increase, but slightly less pronounced than over China. This behaviour is attributed to a combination of emissions associated with increasing urbanization, coupled with a growing industrial production, and the increasing desertification and the resulting increase in dust being transported over Asia.

In the Western USA (region 9), the trend observed by MODIS (Aqua) from 2003 to 2008 shows an increase in apparent disagreement with the trends derived from the other instruments. Lower rainfall and resultant enhanced fire activity (see Fig. 9), which occurred over parts of the Western USA from 2003 to 2008 (La Niña phases) (Westerling et al., 2006), qualitatively provides an expansion of the difference. As wildfires typically ignite in the afternoon (Mu et al., 2011), the increase, resulting from the fires,

ACPD
13, 26001–26041, 2013

might be much more significant in MODIS (Aqua) AOT, which flies in a sun synchronous orbit with an early afternoon equator crossing time.

Over the Eastern USA (region 10), a decreasing AOT change/trend is generally observed. This behaviour is attributed in large part to the results of legislation and the subsequent measures introduced to reduce pollutant emissions, as reported in previous studies (Streets et al., 2003; Zhao et al., 2008; Yoon et al., 2012; Hilboll et al., 2013). The increasing trend of MODIS (Aqua) AOT in the afternoon is different to the other derived trends. However, it should be noted that the MODIS (Aqua) trends over Eastern USA are not significant in most areas, but only contributed from the significant trends over central USA as shown in Figs. 6d, 7d, and 8.

To investigate further the remarkable behaviour of AOTs over East China (region 6), where the largest aerosol loadings are now observed, the time series of atmospheric AOTs normalized to total means, tropospheric nitrogen dioxide (NO_2) and sulphur dioxide (SO_2) columns from SCIAMACHY (Burrows et al., 1995; Richter et al., 2005; Bovensmann et al., 1999; Hilboll et al., 2013), and Chinese GDP (The World Bank Group, 2012) are compared in Fig. 10 from 2003 to 2008. This period is chosen because all the data sets are available. In spite of having different temporal samplings and retrieval algorithms, the relative behaviour of the AOTs retrieved from the set of satellite instruments are all in reasonable agreement with each other and the ground-based observations, e.g. the AERONET AOTs measured in Beijing. The AOT trends over East China in spring, summer, autumn, winter are up to +2.53 %, +3.25 %, +3.26 % and +3.58 % yr^{-1} from 2003 to 2008, respectively.

As is now well established the atmospheric oxidation of SO_2 produces sulphuric acid, H_2SO_4. This has low volatility but is highly hygroscopic, and thus an ideal cloud condensation nucleus (Wallace and Hobbs, 2006). The oxidation of NO_2 produces nitric acid, which has a high solubility, and is absorbed by tropospheric aerosol (Pozzoli et al., 2008). The SO_2 and NO_2 seasonal cycles reflect changes in their atmospheric lifetimes, the amount and type of fossil fuel combustion, and seasonal advection patterns. SO_2 has a strong temporal correlation with the fine-mode aerosol loading in winter (i.e.

ACPD
13, 26001–26041, 2013

correlation coefficient $R = 0.6$ between SCIAMACHY SO_2 and AERONET fine-mode dominant AOT at Beijing (Yoon et al., 2012), see Fig. 11, which shows how well they are correlated), when mineral dust from Asian deserts over East China is low. Winter trends of +22.41 % yr^{-1} for fine-mode dominant aerosols in Beijing and +9.32 % yr^{-1} for SO_2 over East China from 2003 to 2008 are obtained.

The maximum aerosol loading over China occurs in spring and early summer. This is the dry and windy season when mineral dust is transported by westerly winds from the Asian deserts. The MISR AOTs over the Asian deserts are strongly correlated to the other three independent AOTs over East Asia (i.e. the correlation ranges from 0.8 to 0.9, as shown in Fig. 12). A significant increase of atmospheric aerosol in spring is observed in all datasets, which varies from +0.94 to +2.53 % yr^{-1}. This is attributed to the growth of the Asian desert (Jeong et al., 2011) and thus desert dust, accompanied by reduced precipitation, approximately −5.62 % yr^{-1} estimated from NCEP/NCAR reanalysis data (NOAA Earth System Research Laboratory, 2012). These processes, which may be both in part a natural phenomena and in part induced by anthropogenic activity, result in an increase in desert dust aerosol, acting as a surface for deposition of pollutants, over the populated regions of China, Korea and Japan as well as the amount transported to the Pacific and beyond.

7 Conclusions and outlook

By using a new trend model (i.e. weighted least squares regression) and optimally different measurements (MODIS-Terra, MISR-Terra, SeaWiFS-OrbView-2, and MODIS-Aqua) from 1998 to 2010, we have established a benchmark for the rate of change of AOT in selected regions. The uncertainty in the trend analysis induced from the cloud disturbance and different/limited temporal sampling has been discussed for the first time, and successfully minimized in this study. The dramatic increases in AOT, associated with rapid industrial growth and desertification are clearly identified. The positive impact of legislation in reducing AOT and improving air quality is unambiguously docu-

ACPD
13, 26001–26041, 2013

mented in the developed world (Zhao et al., 2008; Yoon et al., 2011, 2012; Hsu et al., 2012; de Meij et al., 2012). This is an optimistic sign that mitigation of anthropogenic activity, when introduced, is having the intended consequence of reducing a threat to human health. In contrast, regions with uncontrolled pollutant emissions, associated with rapid economic growth and impacted by desertification have increasing trends in AOT. These changes are certainly able to influence the global climate change, and therefore the further studies are needed to investigate the consequence.

The recent severe smog in China during the winter 2012/2013 is a dramatic consequence of the emissions from economic growth, as shown by the increases in gross domestic product shown in Fig. 10, coupled with minimal environmental legislation. This trend is only mildly influenced by the recent global economic crisis, which began in 2008, and the cleaning up operation for the 2008 Olympics including introduction of desulfurization in coal fired power plants. How the atmospheric aerosol loading will evolve in a polluted and warming climate is not yet clear. Measurements of the type described in this study and better are required to assess objectively the changes. The generation of pioneering space-based remote sensing instrumentation is near to, or at its end of life. New and improved systems are required urgently to provide continuity and improved knowledge in the next phase of the anthropocene, uniquely enabling early warning of the direction and magnitude of these changes, and testing our understanding of the sources, sinks and processing of aerosol in the troposphere. The data products form such a constellation of instruments and data products simultaneously provide an evidence base for international environmental policymaking, addressing the key short-lived climate substances (CCAC, 2012), which impact on human health, agriculture, food security, ecosystem services and climate change.

Acknowledgements. The authors would like to thank NASA and NOAA ESRL teams for providing AERONET, MODIS, MISR AOT data, SeaWiFS upwelling reflectance, and NCEP/NCAR reanalysis data. This work was supported in part by the CityZen project (megacity – Zoom for the Environment: EU Framework Programme 7 of European Commission), the DFG Project Terra, and the State and University of Bremen.

ACPD
13, 26001–26041, 2013

References

Barnes, R. A., Eplee Jr., R. E., Schmidt, G. M., Patt, F. S., and Mc-Clain, C. R.: Calibration of SeaWiFS, I: direct techniques, Appl. Optics, 40, 6682–6700, doi:10.1364/AO.40.006682, 2001.

Basart, S., Pérez, C., Cuevas, E., Baldasano, J. M., and Gobbi, G. P.: Aerosol characterization in Northern Africa, Northeastern Atlantic, Mediterranean Basin and Middle East from direct-sun AERONET observations, Atmos. Chem. Phys., 9, 8265–8282, doi:10.5194/acp-9-8265-2009, 2009.

Bovensmann, H., Burrows, J. P., Buchwitz, M., Frerick, J., Noël, S., Rozanov, V. V., Chance, K. V., and Goede, A. P. H.: SCIAMACHY – mission objectives and measurement modes, J. Atmos. Sci., 56, 127–150, doi:10.1175/1520-0469(1999)056<0127:SMOAMM>2.0.CO;2, 1999.

Burrows, J. P., Hölzle, E., Goede, A. P. H., Visser, H., and Fricke, W.: SCIAMACHY – Scanning Imaging Absorption Spectrometer for Atmospheric Chartography, Acta Astronaut., 35, 445–451, 1995.

Bruegge, C. J., Diner, D. J., Kahn, R. A., Chrien, N., Helmlinger, M. C., Gaitley, B. J., and Abdou, W. A.: The MISR radiometric calibration process, Remote Sens. Environ., 107, 2–11, doi:10.1016/j.rse.2006.07.024, 2007.

Climate and Clean Air Coalition (CCAC): Short-lived climate pollutants, available at: http://www.unep.org/ccac/ShortLivedClimatePollutants/tabid/101650/Default.aspx, 2012.

de Meij, A., Pozzer, A., and Lelieveld, J.: Trend analysis in aerosol optical depths and pollutant emission estimates between 2000 and 2009, Atmos. Environ., 51, 75–85, doi:10.1016/j.atmosenv.2012.01.059, 2012.

de Ruyter de Wildt, M., Eskes, H., and Boersma, K. F.: The global economic cycle and satellite-derived NO_2 trends over shipping lanes, Geophys. Res. Lett., 39, L01802, doi:10.1029/2011GL049541, 2012.

Dey, S., Tripathi, S. N., Singh, R. P., and Holben, B. N.: Influence of dust storms on the aerosol optical properties over the Indo-Gangetic plains, J. Geophys. Res., 109, D20211, doi:10.1029/2004JD004924, 2004.

Dubovik, O., Holben, B. N., Eck, T. F., Smirnov, A., Kaufman, Y. J., King, M. D., Tanré, D., and Slutsker, I.: Variability of absorption and optical properties of key aerosol

ACPD
13, 26001–26041, 2013

types observed in worldwide locations, J. Atmos. Sci., 59, 590–608, doi:10.1175/1520-0469(2002)059<0590:VOAAOP>2.0.CO;2, 2002.
Eck, T. F., Holben, B. N., Reid, J. S., Dubovik, O., Smirnov, A., O'Neill, N. T., Slutsker, I., and Kinne, S.: Wavelength dependence of the optical depth of biomass burning, urban, and desert dust aerosol, J. Geophys. Res., 104, 31333–31349, doi:10.1029/1999JD900923, 1999.
Eplee Jr., R. E., Robinson, W. D., Bailey, S. W., Clark, D. K., Werdell, P. J., Wang, M., Barnes, R. A., and McClain, C. R.: The calibration of SeaWiFS, Part 2: vicarious techniques, Appl. Optics, 40, 6701–6718, doi:10.1364/AO.40.006701, 2001.
Franke, K., Richter, A., Bovensmann, H., Eyring, V., Jöckel, P., Hoor, P., and Burrows, J. P.: Ship emitted NO_2 in the Indian Ocean: comparison of model results with satellite data, Atmos. Chem. Phys., 9, 7289–7301, doi:10.5194/acp-9-7289-2009, 2009.
Giglio, L., Randerson, J. T., van der Werf, G. R., Kasibhatla, P. S., Collatz, G. J., Morton, D. C., and DeFries, R. S.: Assessing variability and long-term trends in burned area by merging multiple satellite fire products, Biogeosciences, 7, 1171–1186, doi:10.5194/bg-7-1171-2010, 2010.
Goddard Space Flight Center – NASA: SeaWiFS Project, available at: http://oceancolor.gsfc.nasa.gov/SeaWiFS, 1997.
Goldman Sachs: Dreaming With BRICs: The Path to 2050, Global Economics Paper No. 99, Goldman Sachs, 2003.
Gordon, H. R.: In-orbit calibration strategy for ocean color sensors, Remote Sens. Environ., 63, 265–278, 1998.
Grubbs, F.: Procedures for detecting outlying observations in samples, Technometrics, 11, 1–21, 1969.
Hayn, M., Beirle, S., Hamprecht, F. A., Platt, U., Menze, B. H., and Wagner, T.: Analysing spatio-temporal patterns of the global NO_2-distribution retrieved from GOME satellite observations using a generalized additive model, Atmos. Chem. Phys., 9, 6459–6477, doi:10.5194/acp-9-6459-2009, 2009.
Hilboll, A., Richter, A., and Burrows, J. P.: Long-term changes of tropospheric NO_2 over megacities derived from multiple satellite instruments, Atmos. Chem. Phys., 13, 4145–4169, doi:10.5194/acp-13-4145-2013, 2013.
Holben, B. N., Eck, T. F., Slutsker, I., Tanré,v, Buis, J. P., Setzer, A., Vermote, E., Reagan, J. A., Kaufman, Y., Nakajima, T., Lavenu, F., Jankowiak, I., and Smirnov, A.: AERONET – a feder-

ACPD
13, 26001–26041, 2013

ated instrument network and data archive for aerosol characteristics, Remote Sens. Environ., 66, 1–16, doi:10.1016/S0034-4257(98)00031-5, 1998.
Holben, B. N., Tanré, D., Smirnov, A., Eck, T. F., Slutsker, I., Abuhassan, N., Newcomb, W. W., Schafer, J. S., Chatenet, B., Lavenu, F., Kaufman, Y. J., Vande Castle, J., Setzer, A., Markham, B., Clark, D., Frouin, R., Halthore, R., Karneli, A., O'Neill, N. T., Pietras, C., Pinker, R. T., Voss, K., and Zibordi, G.: An emerging ground-based aerosol climatology: Aerosol optical depth from AERONET, J. Geophys. Res., 106, 12067–12097, doi:10.1029/2001JD900014, 2001.
Hsu, N. C., Gautam, R., Sayer, A. M., Bettenhausen, C., Li, C., Jeong, M. J., Tsay, S.-C., and Holben, B. N.: Global and regional trends of aerosol optical depth over land and ocean using SeaWiFS measurements from 1997 to 2010, Atmos. Chem. Phys., 12, 8037–8053, doi:10.5194/acp-12-8037-2012, 2012.
Ignatov, A., Minnis, P., Loeb, N., Wielicki, B., Miller, W., Sun-Mack, S., Tanré, S., Remer, L., Laszlo, I., and Geier, E.: Two MODIS aerosol products over ocean on the terra and aqua CERES SSF datasets, J. Atmos. Sci., 62, 1008–1031, doi:10.1175/JAS3383.1, 2005.
Jeong, S.-J., Ho, C.-H., Brown, M. E., Kug, J.-S., and Piao, S.: Browning in desert boundaries in Asia in recent decades, J. Geophys. Res., 116, D02103, doi:10.1029/2010JD014633, 2011.
Jet Propulsion Laboratory – NASA: MISR Multiangle Imaging SpectroRadiometer, available at: http://www-misr.jpl.nasa.gov, 2000.
Kahn, R. A., Li, W.-H., Martonchik, J., Bruegge, C., Diner, D., Gaitley, B., Abdou, W., Dubovik, O., Holben, B., Smirnov, S., Jin, Z., and Clark, D.: MISR low-light-level calibration, and implications for aerosol retrieval over dark water, J. Atmos. Sci., 62, 1032–1062, doi:10.1175/JAS3390.1, 2005a.
Kahn, R. A., Gaitley, B., Martonchik, J., Diner, D., Crean, K., and Holben, B.: MISR global aerosol optical depth validation based on two years of coincident AERONET observations, J. Geophys. Res., 110, D10S04, doi:10.1029/2004JD004706, 2005b.
Kahn, R. A., Garay, M., Nelson, D., Yau, K., Bull, M., and Martonchik, J.: Satellite-derived aerosol optical depth over dark water from MISR and MODIS: comparisons with AERONET and implications for climatological studies, J. Geophys. Res., 112, D18205, doi:10.1029/2006JD008175, 2007.
Kahn, R. A., Gaitley, B. J., Garay, M. J., Diner, D. J., Eck, T. F., Smirnov, A., and Holben, B. N.: Multiangle Imaging SpectroRadiometer global aerosol product assess-

ACPD
13, 26001–26041, 2013

ment by comparison with the Aerosol Robotic Network, J. Geophys. Res., 25, D23209, doi:10.1029/2010JD014601, 2010.
Karnieli, A., Derimian, Y., Indoitu, R., Panov, N., Levy, R. C., Remer, L. A., Maenhaut, W., and Holben, B. N.: Temporal trend in anthropogenic sulfur aerosol transport from Central and Eastern Europe to Israel, J. Geophys. Res., 114, D00D19, doi:10.1029/2009JD011870, 2009.
Kaufman, Y. J., Tanré, D., Remer, L. A., Vermote, E. F., Chu, A., and Holben, B. N.: Operational remote sensing of tropospheric aerosol over land from EOS moderate resolution imaging spectroradiometer, J. Geophys. Res., 102, 17051–17068, 1997.
Levy, R. C., Leptoukh, G. G., Kahn, R., Zubko, V., Gopalan, A., and Remer, L. A.: A critical look at deriving monthly aerosol optical depth from satellite data, IEEE T. Geosci. Remote, 47, 2942–2956, doi:10.1109/TGRS.2009.2013842, 2009.
Levy, R. C., Remer, L. A., Kleidman, R. G., Mattoo, S., Ichoku, C., Kahn, R., and Eck, T. F.: Global evaluation of the Collection 5 MODIS dark-target aerosol products over land, Atmos. Chem. Phys., 10, 10399–10420, doi:10.5194/acp-10-10399-2010, 2010.
Li, Z., Zhao, X., Kahn, R., Mishchenko, M., Remer, L., Lee, K.-H., Wang, M., Laszlo, I., Nakajima, T., and Maring, H.: Uncertainties in satellite remote sensing of aerosols and impact on monitoring its long-term trend: a review and perspective, Ann. Geophys., 27, 2755–2770, doi:10.5194/angeo-27-2755-2009, 2009.
Massie, T. S., Torres, O., and Smith, S. J.: Total ozone mapping spectrometer (TOMS) observations of increases in Asian aerosol in winter from 1979 to 2000, J. Geophys. Res., 109, D18211, doi:10.1029/2004JD004620, 2004.
Marmer, E., Langmann, B., Fagerli, H., and Vestreng, V.: Direct shortwave radiative forcing of sulphate aerosol over Europe from 1900 to 2000, J. Geophys. Res., 112, D23S17, doi:10.1029/2006JD008037, 2007.
Meehl, G. A., Covey, C., Delworth, T., Latif, M., McAvaney, B., Mitchell, J. F. B., Stouffer, R. J., and Taylor, K. E.: The WCRP CMIP3 multimodel dataset: a new era in climate change research, B. Am. Meteorol. Soc., 88, 1383–1394, doi:10.1175/BAMS-88-9-1383, 2007.
Mishchenko, M. and Geogdzhayev, I. V.: Satellite remote sensing reveals regional tropospheric aerosol trends, Opt. Express, 15, 7423–7438, doi:10.1364/OE.15.007423, 2007.
Mishchenko, M., Geogdzhayev, I. V., Rossow, W. B., Cairns, B., Carlson, B. E., Lacis, A. A., Liu, L., and Travis, L. D.: Long-term satellite record reveals likely recent aerosol trend, Science, 315, 1543, doi:10.1126/science.1136709, 2007.

ACPD
13, 26001–26041, 2013

Mu, M., Randerson, J. T., van der Werf, G. R., Giglio, L., Kasibhatla, P., Morton, D., Collatz, G. J., DeFries, R. S., Hyer, E. J., Prins, E. M., Griffith, D. W. T., Wunch, D., Toon, G. C., Sherlock, V., and Wennberg, P. O.: Daily and 3-hourly variability in global fire emissions and consequences for atmospheric model predictions of carbon monoxide, J. Geophys. Res., 116, D24303, doi:10.1029/2011JD016245, 2011.

Mudelsee, M.: Climate Time Series Analysis: Classical Statistical and Bootstrap Methods (Atmospheric and Oceanographic Sciences Library), Springer, Dordecht, Heildelberg, London, and New York, 74–77, ISBN:978-9048194810, 2010.

National Aeronautics and Space Administration (NASA): MODIS Web, available at: http://modis.gsfc.nasa.gov, 2000.

NOAA Earth System Research Laboratory: NCEP/NCAR Reanalysis Monthly Means and Other Derived Variables, available at: http://www.esrl.noaa.gov/psd/data/gridded/data.ncep.reanalysis.derived.html, 2012.

Pozzoli, L., Bey, I., Rast, S., Schultz, M. G., Stier, P., and Feichter, J.: Trace gas and aerosol interactions in the fully coupled model of aerosol–chemistry–climate ECHAM5-HAMMOZ: 1. model description and insights from the spring 2001 TRACE-P experiment, J. Geophys. Res., 113, D07308, doi:10.1029/2007JD009007, 2008.

Ramanathan, V., Li, F., Ramana, M. V., Praveen, P. S., Kim, D., Corrigan, C. E., Nguyen, H., Stone, E. A., Schauer, J. J., Carmichael, G. R., Adhikary, B., and Yoon, S. C.: Atmospheric brown clouds: hemispherical and regional variations in long-range transport, absorption, and radiative forcing, J. Geophys. Res., 112, D22S21, doi:10.1029/2006JD008124, 2007a.

Ramanathan, V., Ramana, M. V., Roberts, G., Kim, D., Corrigan, C., Chung, C., and Winker, D.: Warming trends in Asia amplified by brown cloud solar absorption, Nature Lett., 448, 575–578, doi:10.1038/nature06019, 2007b.

Remer, L. A., Gasso, S., Hegg, D. A., Kaufman, Y. J., and B. N. Holben: Urban/industrial aerosol: ground-based sun/sky radiometer and airborne in situ measurements, J. Geophys. Res., 102, 16849–16859, doi:10.1029/96JD01932, 1997.

Remer, L. A., Kaufman, Y. J., Tanré, D., Mattoo, S., Chu, D. A., Martins, J. V., Li, R.-R., Ichoku, C., Levy, R. C., Kleidman, R. G., Eck, T. F., Vermote, E., and Holben, B. N.: The MODIS aerosol algorithm, products, and validation, J. Atmos. Sci., 62, 947–973, doi:10.1175/JAS3385.1, 2005.

ACPD
13, 26001–26041, 2013

Remer, L. A., Kleidman, R. G., Levy, R. C., Kaufman, Y. J., Tanré, D., Mattoo, S., Martins, J. V., Ichoku, C., Koren, I., Yu, H., and Holben, B. N.: Global aerosol climatology from the MODIS satellite sensors, J. Geophys. Res., 113, D14S07, doi:10.1029/2007JD009661, 2008.
Richter, A., Eyring, V., Burrows, J. P., Bovensmann, H., Lauer, A., Sierk, B., and Crutzen, P. J.: Satellite measurements of NO_2 from international shipping emissions, Geophys. Res. Lett., 31, L23110, doi:10.1029/2004GL020822, 2004.
Richter, A., Burrows, J. P., Nüß, H., Granier, C., and Niemeier, U.: Increase in tropospheric nitrogen dioxide over China observed from space, Nature Lett., 437, 129–132, doi:10.1038/nature04092, 2005.
Sabbah, I., Saeed, T., Al Jassar, H. K., and Rao, K. S.: Remote sensing of desert dust in Kuwait, J. Sci. Eng., 33, 101–117, 2006.
Sadrinasab, M. and Kämpf, J.: Three-dimensional flushing times of the Persian Gulf, Geophys. Res. Lett., 31, L24301, doi:10.1029/2004GL020425, 2004.
Smirnov, A., Holben, B. N., Eck, T. F., Slutsker, I., Chatenet, B., and Pinker, R. T.: Diurnal variability of aerosol optical depth observed at AERONET (Aerosol Robotic Network) sites, Geophys. Res. Lett., 29, 30-1–30-4, doi:10.1029/2002GL016305, 2002.
Solomon, S., Qin, D., Manning, M., Chen, Z., Marquis, M., Averyt, K. B., Tignor, M., and Miller, H. L.: Climate Change 2007, The Physical Science Basis – Contribution of Working Group I to the Fourth Assessment Report of the Intergovernmental Panel on Climate Change (IPCC), Cambridge University Press, Cambridge, UK and New York, USA, ISBN:9780521705967, 2007.
Streets, D. G., Bond, T. C., Carmichael, G. R., Fernandes, S. D., Fu, Q., He, D., Klimont, Z., Nelson, S. M., Tsai, N. Y., Wang, M. Q., Woo, J. -H., and Yarber, K. F.: An inventory of gaseous and primary aerosol emissions in Asia in the year 2000, J. Geophys. Res., 108, D21, 8809, doi:10.1029/2002JD003093, 2003.
Streets, D. G., Wu, Y., and Chin, M.: Two-decadal aerosol trends as a likely explanation of the global dimming/brightening transition, Geophys. Res. Lett., 33, L15806, doi:10.1029/2006GL026471, 2006.
Taylor, K. E.: Summarizing multiple aspects of model performance in a single diagram, J. Geophys. Res., 106, 7183–7192, doi:10.1029/2000JD900719, 2001.
The World Bank Group: The World Bank Data, available at: http://data.worldbank.org/, 2012.
Thomas, G. E., Poulsen, C. A., Siddans, R., Sayer, A. M., Carboni, E., Marsh, S. H., Dean, S. M., Grainger, R. G., and Lawrence, B. N.: Validation of the GRAPE single view aerosol retrieval

ACPD
13, 26001–26041, 2013

for ATSR-2 and insights into the long term global AOD trend over the ocean, Atmos. Chem. Phys., 10, 4849–4866, doi:10.5194/acp-10-4849-2010, 2010.

von Hoyningen-Huene, W., Freitag, M., and Burrows, J. P.: Retrieval of aerosol optical thickness over land surfaces from top-of-atmosphere radiance, J. Geophys. Res., 108, D94260, doi:10.1029/2001JD002018, 2003.

von Hoyningen-Huene, W., Kokhanovsky, A. A., Burrows, J. P., Bruniquel-Pinel, V., Regner, P., and Baret, F.: Simultaneous determination of aerosol- and surface characteristics from top-of-atmosphere reflectance using MERIS on board of ENVISAT, J. Adv. Space Res., 37, 2172–2177, doi:10.1016/j.asr.2006.03.017, 2006.

von Hoyningen-Huene, W., Yoon, J., Vountas, M., Istomina, L. G., Rohen, G., Dinter, T., Kokhanovsky, A. A., and Burrows, J. P.: Retrieval of spectral aerosol optical thickness over land using ocean color sensors MERIS and SeaWiFS, Atmos. Meas. Tech., 4, 151–171, doi:10.5194/amt-4-151-2011, 2011.

Wallace, J. M. and Hobbs, P. V.: Atmospheric Chemistry, in: Atmospheric Science: An Introductory Survey, 2nd edn., edited by: Dmowska, R., Hartmann, D., and Rossby, H. T., Elsevier, MA, USA, California, USA, and London, UK, 153–207, 2006.

Weatherhead, E. C., Reinsel, G. C., Tiao, G. C., Meng, X.-L., Choi, D., Cheang, W.-K., Keller, T., DeLuisi, J., Wuebbles, D. J., Kerr, J. B., Miller, A. J., Oltmans, S. J., and Frederick, J. E.: Factors affecting the detection of trends: statistical considerations and applications to environmental data, J. Geophys. Res., 103, 17149–17161, doi:10.1029/98JD00995, 1998.

Westerling, A. L., Hidalgo, H. G., Cayan, D. R., and Swetnam, T. W.: Warming and earlier spring increase Western US forest wildfire activity, Science, 313, 940–943, doi:10.1126/science.1128834, 2006.

World Meteorological Organization (WMO): Systematic observation requirements for satellite-based products for climate supplemental details to the satellite-based component of the implementation plan for the global observing system for climate in support of the UNFCCC-2011 update, GCOS, 154, 1–127, 2011.

World Health Organization (WHO): Health Topics, Air Pollution, available at: http://www.who.int/topics/air_pollution/en/, 2012.

Yoon, J., von Hoyningen-Huene, W., Vountas, M., and Burrows, J. P.: Analysis of linear long-term trend of aerosol optical thickness derived from SeaWiFS using BAER over Europe and South China, Atmos. Chem. Phys., 11, 12149–12167, doi:10.5194/acp-11-12149-2011, 2011.

ACPD
13, 26001–26041, 2013

Yoon, J., von Hoyningen-Huene, W., Kokhanovsky, A. A., Vountas, M., and Burrows, J. P.: Trend analysis of aerosol optical thickness and Ångström exponent derived from the global AERONET spectral observations, Atmos. Meas. Tech., 5, 1271–1299, doi:10.5194/amt-5-1271-2012, 2012.

Yu, H., Chin, M., Remer, L. A., Kleidman, R. G., Bellouin, N., Bian, H., and Diehl, T.: Variability of marine aerosol fine-mode fraction and estimates of anthropogenic aerosol component over cloud-free oceans from the Moderate Resolution Imaging Spectroradiometer (MODIS), J. Geophys. Res., 114, D10206, doi:10.1029/2008JD010648, 2009.

Zhang, J. and Reid, J. S.: A decadal regional and global trend analysis of the aerosol optical depth using a data-assimilation grade over-water MODIS and Level 2 MISR aerosol products, Atmos. Chem. Phys., 10, 10949–10963, doi:10.5194/acp-10-10949-2010, 2010.

Zhang, X. Y., Gong, S. L., Zhao, T. L., Arimoto, R., Wang, T. Q., and Zhou, Z. J.: Sources of Asian dust and role of climate change versus desertification in Asian dust emission, Geophys. Res. Lett., 30, 24, 2272, doi:10.1029/2003GL018206, 2003.

Zhao, T. X.-P., Laszlo, I., Guo, W., Heidinger, A., Cao, C., Jelenak, A., Tarpley, D., and Sullivan, J.: Study of long-term trend in aerosol optical thickness observed from operational AVHRR satellite instrument, J. Geophys. Res., 113, D07201, doi:10.1029/2007JD009061, 2008.

Zhou, Y., Brunner, D., Hueglin, C., Henne, S., and Staehelin, J.: Changes in OMI tropospheric NO_2 columns over Europe from 2004 to 2009 and the influence of meteorological variability, Atmos. Environ., 46, 482–495, doi:10.1016/j.atmosenv.2011.09.024, 2012.

ACPD
13, 26001–26041, 2013

Table 1. The characteristics of the sensors and polar-orbiting satellites, used in this study, the sensor calibration approaches, aerosol retrieval accuracies, and data sets.

Sensor	MODIS (Moderate Resolution Imaging Spectroradiometer)		MISR (Multi-angle Imaging SpectroRadiometer)	SeaWiFS (Sea-viewing Wide Field-of-view Sensor)
Satellite	Terra	Aqua	Terra	OrbView-2
Local Equatorial Crossing Time	10.30 a.m.	001.30 p.m.	10.30 a.m.	12.20 p.m.
Launch Date	18 Dec 1999	4 May 2002	18 Dec 1999	1 Aug 1997
Orbit	Descending node	Ascending node	Descending node	Descending node
Swath (km)	2330		360	2801 (LAC) 1502 (GAC)
Resolution (m)	250 (bands 1–2) 500 (bands 3–7) 1000 (bands 8–36)		250	1100 (LAC) 4500 (LAC)
Number of Bands	36		4	8
Spectral Coverage (nm)	405–14 385		446–867	402–885
View Angles (°)	nadir		0, ±26.1, ±45.6, ±60.0, and ±70.5	nadir
Reference Source	National Aeronautics and Space Administration (NASA), MODIS Web (2000), Jet Propulsion Laboratory – NASA, MISR Multiangle Imaging SpectroRadiometer (2000), Goddard Space Flight Center – NASA, SeaWiFS Project (1997), The International Ocean-Colour Coordinating Group (IOCCG) (2011)			
Sensor Calibration Method	On-board, Vicarious, and Lunar		On-board, Vicarious, and Lunar	On-board, Vicarious, Lunar, Comparison with situ
Calibration Accuracy or Precision	~ 2 % absolute, ~ 1 % precision		~ 3 % absolute, 1–2 % channel-to-channel relative, 1 % precision	0.5 % accuracy, ~ 0.3 % precision
Reference Source	Kahn et al. (2005a), Bruegge et al. (2007), Li et al. (2009), Barnes et al. (2001), Gordon (1998), Eplee et al. (2001)			
Aerosol Retrieval Accuracy	±0.05 or ±15 % (Land) and ±0.05 or ±5 % (Ocean)		±0.05 or ±20 % (Land and Ocean)	±0.05 or ±20–25 % (Land and Ocean)
Reference Source	Kaufman et al. (1997), Remer et al. (2005, 2008), Levy et al. (2010)		Kahn et al. (2005b, 2010)	von Hoyningen-Huene et al. (2003, 2006, 2011), Yoon et al. (2011)
Research Periods	Mar 2000–Dec 2009	Jan 2003–Dec 2008	Mar 2000–Dec 2010	Jan 1998–Dec 2007
Research data* Data Type	AOT (550 nm), CF Level 3 Collection 5		AOT (558 nm) Level 3 CGAS-F15	AOT (510 nm) Level 3 Global Product
Data Resolution	1° × 1°		0.5° × 0.5°	1° × 1°

* AOT and CF: Aerosol Optical Thickness and Cloud Fraction in daytime

ACPD
13, 26001–26041, 2013

Table 2. The AERONET stations classified by regional dominant aerosol types (Yoon et al., 2012) for the investigation of temporal pattern correlation in Fig. 2. The AERONET stations are selected using the criterion that the minimum length of the data set is complete five years (Yoon et al., 2012).

AERONET Stations	Geolocations (lat.[°]/lon.[°]/alt.[m])	Research Periods	Dominant Aerosol Type
Avignon	43.93/4.88/32	2001 ~ 2005	Industrial/Biomass Burning
Banizoumbou	13.54/2.66/250	2002 ~ 2008	Desert
Beijing	39.98/116.38/92	2003 ~ 2007	Industrial/Biomass Burning
Dakar	14.39/−16.96/0	2004 ~ 2008	Desert
GSFC	38.99/−76.84/87	1995 ~ 2008	Industrial/Biomass Burning
Ispra	45.80/8.63/235	2001 ~ 2007	Industrial/Biomass Burning
Mauna_Loa	19.54/−155.58/3397	1998 ~ 2009	Free Troposphere
MD_Science_Center	39.28/−76.62/15	2000 ~ 2006	Industrial/Biomass Burning
Mongu	−15.25/23.15/1107	2000 ~ 2004	Desert
Ouagadougou	12.20/−1.40/290	2000 ~ 2004	Desert
SEDE_BOKER	30.86/34.78/480	2003 ~ 2008	Desert
Sevilleta	34.35/−106.89/1477	1998 ~ 2002	Rural
Shirahama	33.69/135.36/10	2003 ~ 2009	Industrial/Biomass Burning
Skukuza	−24.99/31.59/150	2000 ~ 2007	Industrial/Biomass Burning
Solar_Village	24.91/46.40/764	2001 ~ 2007	Desert

ACPD
13, 26001–26041, 2013

Table 3. Geolocations of AERONET stations and research periods of AERONET level 2.0 AOT data for the trend validations in Fig. 5.

AERTONET Stations	Geolocations (lat.[°]/lon.[°]/alt.[m])	Countries	Research Periods	Targets for Trend Validation[b]
Alta_Floresta	−9.87/−56.10/277	Brazil	2001 ~ 2004	MOD, SEA
Avignon	43.93/4.88/32	France	2003 ~ 2005	MOD, MIS, SEA, MYD
Banizoumbou[a]	13.54/2.66/250	Niger	2003 ~ 2008	MIS
Beijing	39.98/116.38/92	China	2004 ~ 2007	MOD, MIS, SEA, MYD
BONDVILLE	40.05/−88.37/212	USA	2002 ~ 2006	MOD, MIS, SEA, MYD
Capo_Verde	16.73/−22.94/60	Sal Island	2005 ~ 2008	MOD, MIS, SEA, MYD
CEILAP-BA	−34.57/−58.50/10	Argentina	2000 ~ 2007	MOD, SEA, MYD
Dakar[a]	14.39/−16.96/0	Senegal	2004 ~ 2007	MIS
Dalanzadgad[a]	43.58/104.42/1470	Mongolia	1999 ~ 2004	MIS
El_Arenosillo	37.11/−6.73/0	Spain	2002 ~ 2005	MOD, MIS, SEA, MYD
GSFC	38.99/−76.84/87	USA	1998 ~ 2008	MOD, MIS, SEA, MYD
Ispra	45.80/8.63/235	Italy	2001 ~ 2007	MOD, MIS, SEA, MYD
Kanpur	26.51/80.23/123	India	2001 ~ 2006	MOD, MIS, SEA, MYD
La_Parguera	17.97/−67.05/12	Puerto Rico	2006 ~ 2009	MOD, MIS, MYD
Mauna_Loa	19.54/−155.58/3397	USA	1998 ~ 2009	MOD, MIS, SEA, MYD
MD_Science_Center	39.28/−76.62/15	USA	2000 ~ 2006	MOD, MIS, SEA, MYD
Mongu	−15.25/23.15/1107	Zambia	1999 ~ 2008	MOD, MIS, SEA, MYD
Ouagadougou[a]	12.20/−1.40/290	Burkina Faso	2000 ~ 2004	MIS
SEDE_BOKER[a]	30.86/34.78/480	Israel	2004 ~ 2008	MIS
Shirahama	33.69/135.36/10	Japan	2002 ~ 2009	MOD, MIS, SEA, MYD
Skukuza	−24.99/31.59/150	South Africa	2001 ~ 2007	MOD, MIS, SEA, MYD
Solar_Village[a]	24.91/46.40/764	Saudi Arabia	2001 ~ 2007	MIS
Venise	45.31/12.51/10	Italy	2000 ~ 2005	MOD, SEA, MYD

[a] The AERONET stations are used for the trend validation of MISR AOT only.
[b] MOD, MIS, SEA, and MYD are abbreviations for MODIS (Terra), MISR (Terra), SeaWiFS (OrbView-2), and MODIS (Aqua).

ACPD
13, 26001–26041, 2013

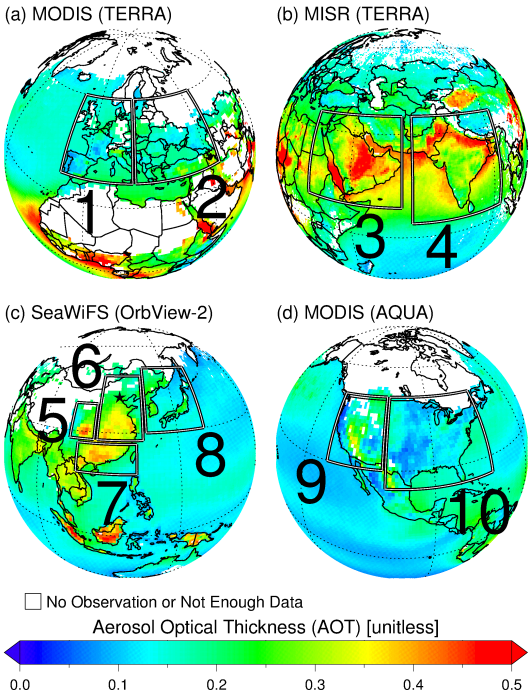

Fig. 1. Plots of the mean values of **(a)** MODIS (Terra) AOT (550 nm) from March 2001 to December 2009, **(b)** MISR (Terra) AOT (558 nm) from March 2001 to December 2010, **(c)** SeaWiFS (OrbView-2) AOT (510 nm) from January 1998 to December 2007, and **(d)** MODIS (Aqua) AOT (550 nm) from January 2003 to December 2008 for the selected regions (1) Western Europe, (2) Eastern Europe, (3) Middle/Near East, (4) South Asia, (5) central China, (6) East China, (7) South China, (8) Korea/Japan, (9) Western USA, and (10) Eastern USA. The latitude/longitude of these regions ranges are shown as numbered rectangles. The black star symbol in region (6) is the location of the AERONET station in Beijing. "No Observation or Not Enough Data" represents the discarded data series, which consist of less than seven monthly data for a year.

ACPD
13, 26001–26041, 2013

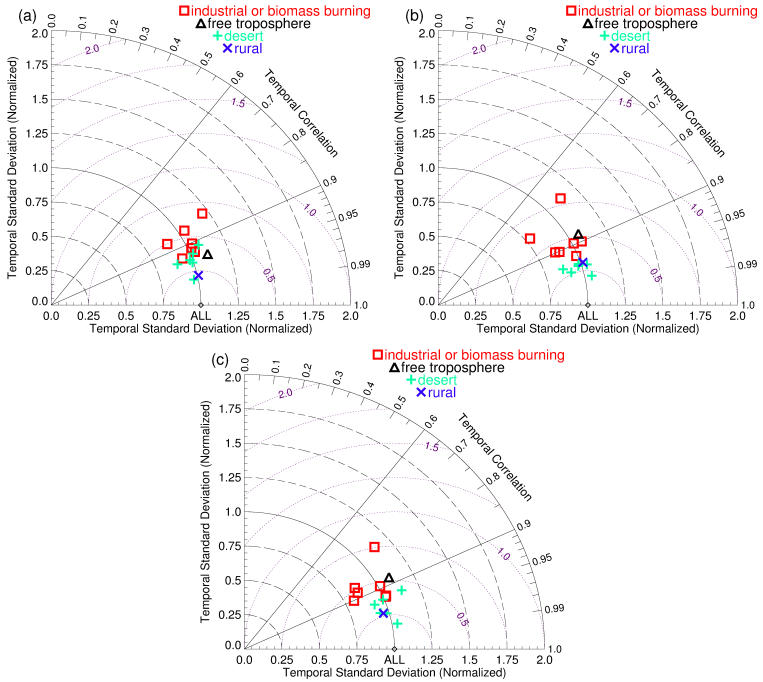

Fig. 2. Taylor diagrams for different sampling times of the different satellite instruments used in this study, all available sampling, **(a)** 10.30 ± 30 a.m., **(b)** 12.20 ± 30 p.m., and **(c)** 001.30 ± 30 p.m. using AERONET AOT (550 nm) data. The normalized centred root-mean-square (RMS) difference is proportional to the distance to the point on the x-axis identified as "ALL" (i.e. shown as purple dashed circles). The AERONET stations are classified by regional dominant aerosol types: industrial/biomass burning, free tropospheric, desert, and rural aerosols (Yoon et al., 2012), and listed in Table 2.

ACPD
13, 26001–26041, 2013

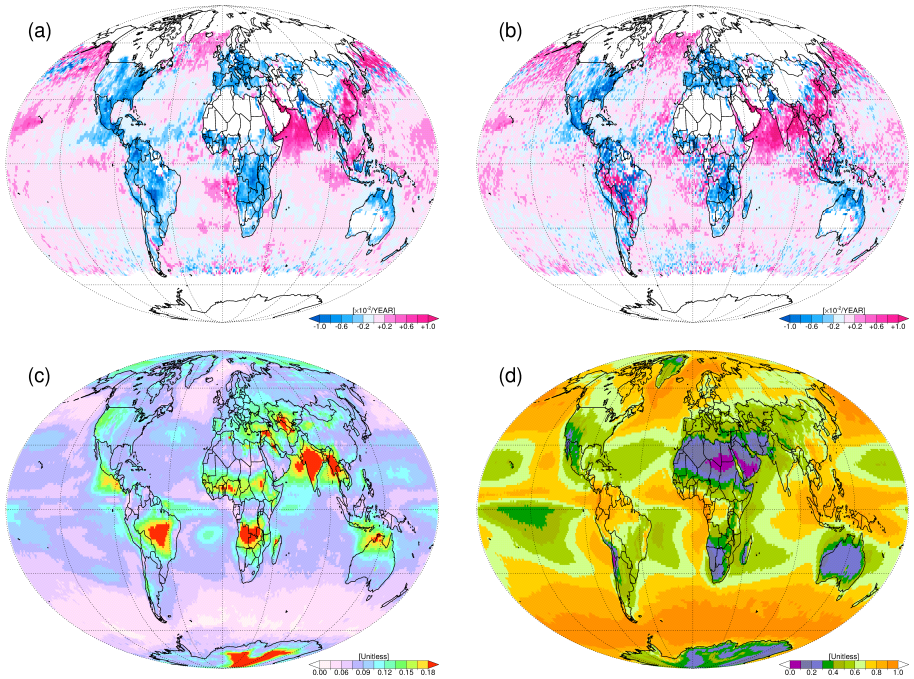

Fig. 3. (a) The simple linear and **(b)** weighted trends of AOT (550 nm) and **(c)** standard deviation and **(d)** total mean of cloud fraction in daytime from MODIS (Terra) observations from March 2001 to December 2009.

ACPD
13, 26001–26041, 2013

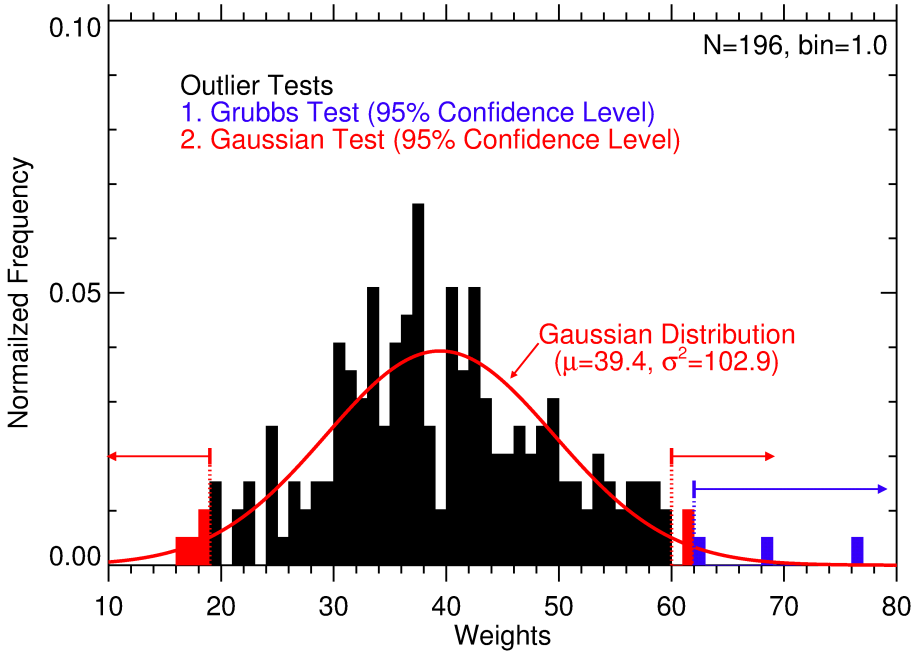

Fig. 4. An example of outlier tests (Grubbs and Gaussian tests) within 95 % of confidence levels. The frequency of weights is normalized to total number (*N*).

ACPD
13, 26001–26041, 2013

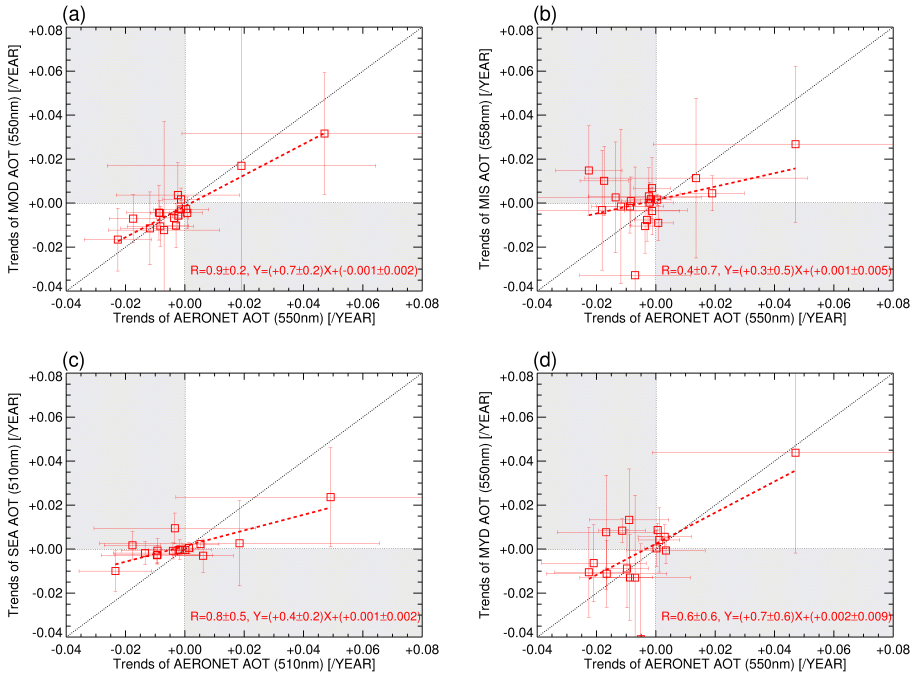

Fig. 5. Scatter plots of comparison between the weighted trends of AERONET and **(a)** MODIS (Terra), **(b)** MISR (Terra), **(c)** SeaWiFS (Orbview-2), and **(d)** MODIS (Aqua) AOTs.

ACPD
13, 26001–26041, 2013

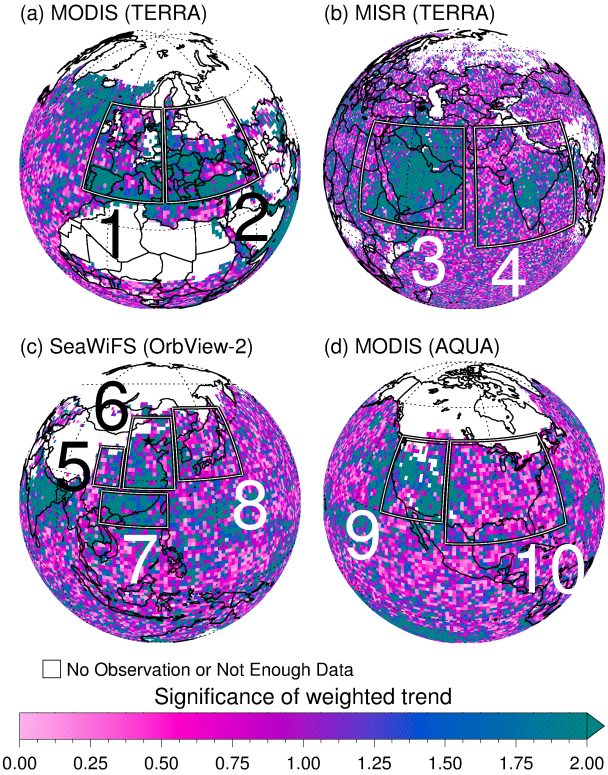

Fig. 6. Plots of the significance of weighted trends derived from **(a)** MODIS (Terra) AOT (550 nm), **(b)** MISR (Terra) AOT (558 nm), **(c)** SeaWiFS (OrbView-2) AOT (510 nm), and **(d)** MODIS (Aqua) AOT (550 nm). The significance is defined as $|B_g/\sigma_{B_g}|$, where B_g and σ_{B_g} are weighted trend and its standard deviation. A significance larger than two means that the trend is statistically significant within 95 % confidence level.

ACPD
13, 26001–26041, 2013

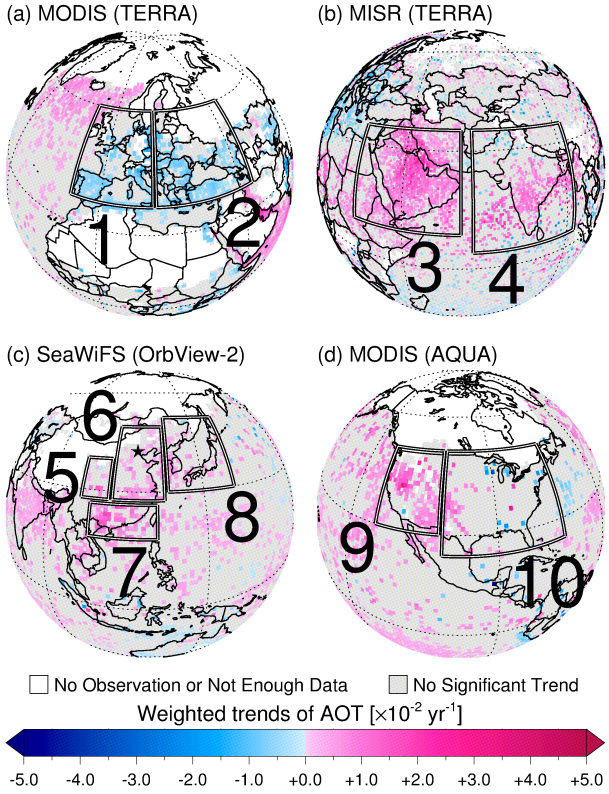

Fig. 7. Weighted trends derived from satellite retrieved AOTs for the selected regions. Each space borne instrument has a different local sampling time; the equatorial crossing times for the satellites are respectively 10.30 a.m. for Terra (descending node), 12.20 p.m. for OrbView-2 (descending node), and 01.30 p.m. for Aqua (ascending node). The weighted trends (B_g) for each grid with significance ($|B_g/\sigma_{B_g}|$) less than two are shown as grey colour representative for not significant trends.

ACPD
13, 26001–26041, 2013

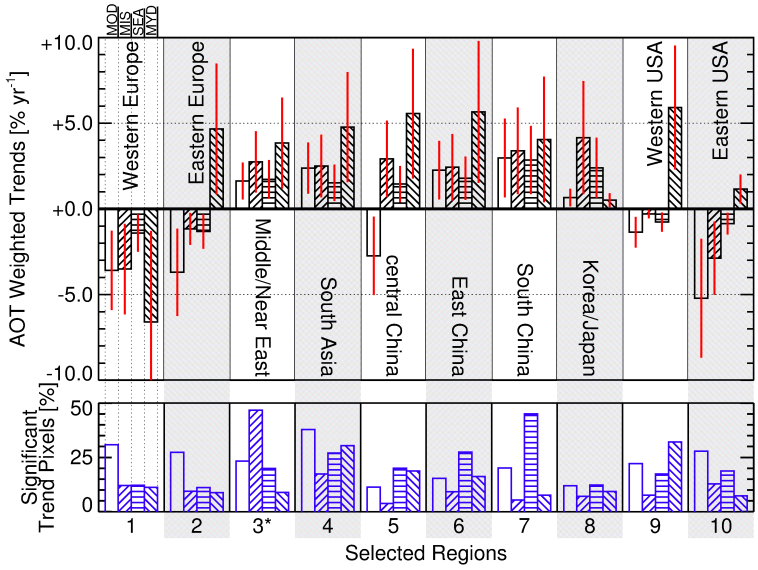

Fig. 8. The relative linear trends and standard deviations ($\pm 2\sigma$) of the four AOT data products, retrieved from the measurements made by MODIS-Terra (MOD), MISR-Terra (MIS), SeaWiFS-OrbView-2 (SEA), and MODIS-Aqua (MYD), for the regions defined in Fig. 5. The standard deviation is attributed to the atmospheric variability and in small part to systematic error in the trend data product. The trends are different because of different release patterns at different sampling times. The regional trends are the mean of the significant weighted trends within 95 % confidence level. The blue bar chart below shows the percentage pixel number of significant trends to all pixels in the selected regions, and thus it represents the central tendency of regional mean. For region 3 (Middle/Near East), only MISR AOTs are available over both land and ocean as a result of the bright surface saturating the measurements by the other instruments.

ACPD
13, 26001–26041, 2013

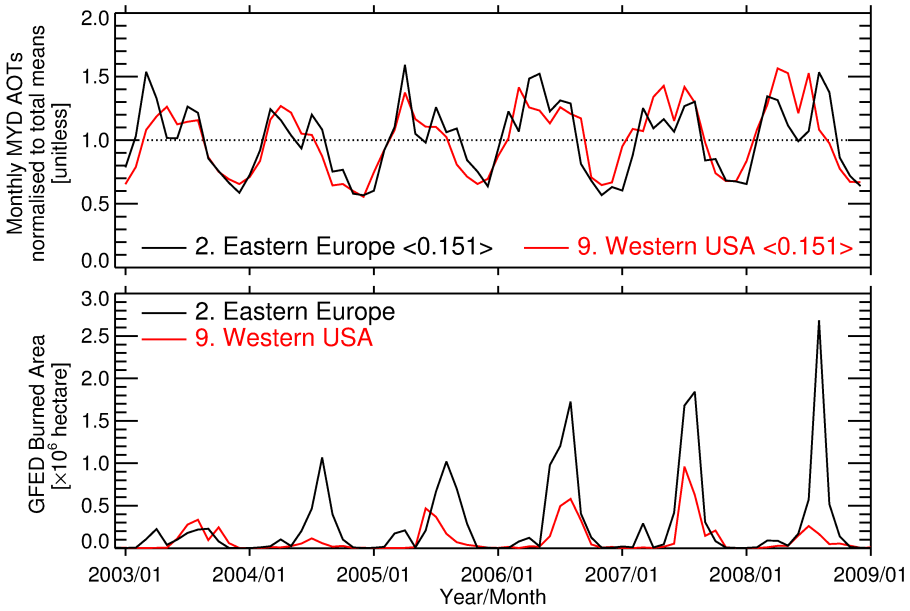

Fig. 9. Plots of the time series of atmospheric AOTs normalized to their average mean values from the data MODIS-Aqua (MYD) and Global Fire Emissions Database (GFED) burned area over Eastern Europe (region 2) and Western USA (region 9) from 2003 to 2008.

ACPD
13, 26001–26041, 2013

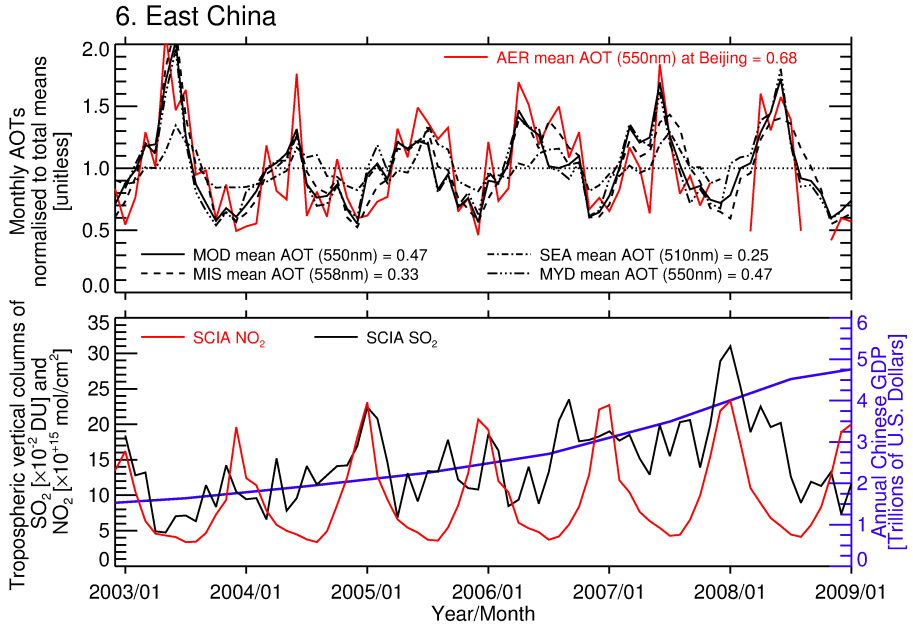

Fig. 10. Plots of the time series of atmospheric AOTs normalised to their average mean values from the data of MODIS-Terra (MOD), MISR-Terra (MIS), SeaWiFS-OrbView-2 (SEA), MODIS-Aqua (MYD), and AERONET (AER), tropospheric nitrogen dioxide and sulphur dioxide columns from SCIAMACHY (SCIA) over East China (region 6), and Chinese GDP from 2003 to 2008.

ACPD
13, 26001–26041, 2013

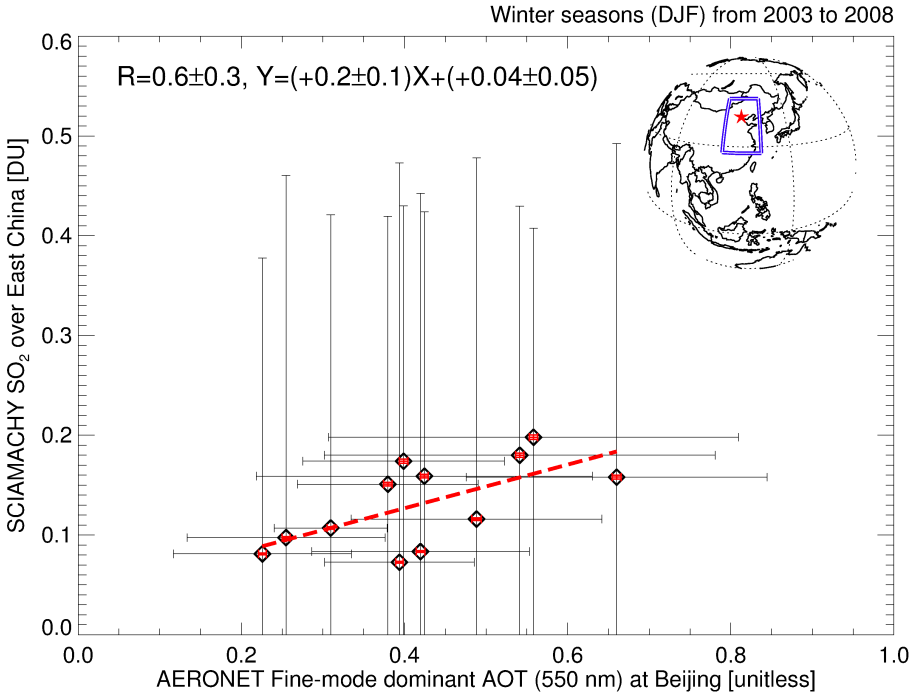

Fig. 11. Plot of the correlation between AERONET fine-mode dominant AOT at Beijing and SCIAMACHY tropospheric SO_2 in winter seasons from 2003 to 2008. Black and red error bars show natural variability and standard retrieval error within 95 % confidence level, respectively.

ACPD
13, 26001–26041, 2013

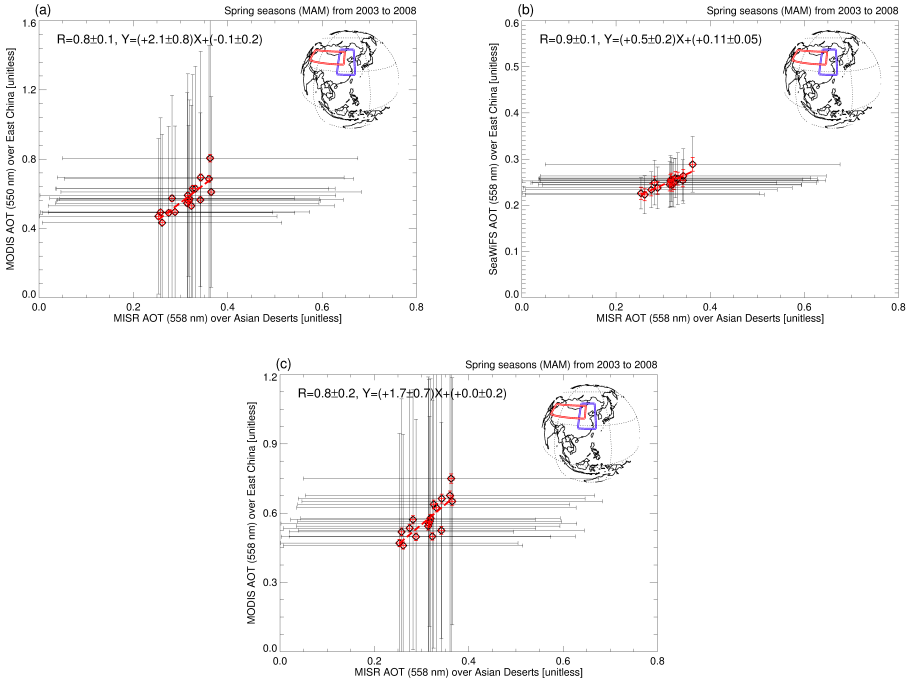

Fig. 12. Plots of the correlations between MISR (Terra) AOT over Asian deserts and independent AOT over East China from 2003 to 2008. **(a)** MODIS (Terra), **(b)** SeaWiFS (OrbView-2), and **(c)** MODIS (Aqua) AOTs. Black and red error bars show natural variability and standard retrieval error within 95 % confidence level, respectively.

ACPD
13, 26001–26041, 2013